JOURNAL OF APPLIED POLYMER SCIENCE VOL. 16, PP. 2877–2899 (1972)

Modifications of the Weissenberg Rheogoniometer for Measurement of Transient Rheological Properties of Molten Polyethylene under Shear. Comparison with Tensile Data*

JOACHIM MEISSNER, *Badische Anilin- and Soda-Fabrik A.G., Mess- und Prüflaboratorium, Ludwigshafen am Rhein, Germany*

Synopsis

Improvements to the Weissenberg rheogoniometer are necessary in order to measure the transient rheological properties of polymer melts correctly. The improvements reported concern the mechanical design, a new heating system, a new normal force measuring system, and additional equipment for the relaxation test. Reliable short-time results require sufficiently stiff torque and normal force springs, and a small radius and relatively large angles of the cone-and-plate gap. The behavior of the LDPE melt under test is "linear viscoelastic," if shear rate or total shear are small: The relaxation modulus, the stress growth at the onset of constant shear rate, the stress relaxation after cessation of steady shear flow, and, in addition, dynamic shear data (from an oscillation viscometer) all show consistent results when correlated by means of formulae from the theory of linear viscoelasticity. Shearing in the nonlinear range with constant shear rate leads to pronounced maxima of the shear stress p_{12} and of the first normal stress difference $p_{11} - p_{22}$ which occur at constant total shear, almost independent of shear rate. Comparison of shear and tensile data (from extensional rheometer) confirms the Trouton relation in the linear-viscoelastic case. In the nonlinear case, there is a "work softening" in shear and a "work hardening" in extension.

INTRODUCTION

In the shear flow of molten polymers, two characteristic features are known: (a) the shear stresses are connected with normal stresses, and (b) at a constant shear rate, the components of the stress tensor are pronounced functions of time.[1]

Until recently, there has been only one instrument commercially available, the Weissenberg rheogoniometer (WRG), which allows the measurement of the "transient" shear and normal stresses to be made, at least in principle.[2] In molten polymers at the onset of a constant strain rate, however, the shear and normal stresses grow so quickly and are so high that the records obtained from the commercial version of the WRG are often a combination of material and of apparatus responses.

* Invited paper presented at the Annual Meeting of the Society of Rheology, Knoxville, Tennessee, October 1971

This paper contains a brief outline of the modifications to the WRG which seem to be necessary and sufficient in order to eliminate the influence of the measuring device on the functions recorded. New and, in our opinion, reliable results concerning the rheological behavior of a low-density polyethylene (LDPE) melt in the linear and the nonlinear range of the viscoelastic deformation are presented. Finally, a comparison is made between the rheological behavior of this material in shear and in extension.

Part of the modification had to be made in order to fulfill the requirements of an international test program of one of the Working Parties of the Macromolecular Division of IUPAC (International Union of Pure and Applied Chemistry). The aim of this Working Party is to establish "relationships of performance characteristics and basic parameters of polymers."[3] In the special test program, three LDPE specimens are compared with respect to (a) molecular characterization, (b) rheological behavior in the molten state, and (c) processing and end use properties.[4] One of the samples is specimen A, which is used in this paper to demonstrate the necessity of the modifications made to the WRG. Specimen A is a low-density polyethylene of melt flow index[5] (MFI) = 1.4 and density (at 20°C) of $\zeta_{20} = 0.918$ g/cm³. All data shown in this paper were obtained at a temperature of 150°C.

THE RHEOGONIOMETER AND GENERAL MODIFICATIONS

The WRG is in principle a cone-and-plate rotational viscometer which operates at constant shear rate $\dot{\gamma}_0$. In addition to the torque, the normal force can be measured which tends to separate the cone and plate when the fluid under test has elastic properties. Because the experimental details of the instrument are already described in the literature,[6] only a brief summary of the vital points of the design need be given here. In this work the Model R 12 of the WRG was used. The model number was changed to R 12/15 after the shaft N of Figure 1 has been replaced by a much thicker one.

Figure 1 is a schematic diagram of the instrument. The rotation of the gallery G with the lower platen (i.e., the cone) is effected by the rotation of the worm wheel WW; and the hollow driving shaft DS. G and DS are connected to each other by means of a special diaphram D which is stiff with respect to rotation but soft with respect to (small) axial movements. Therefore, the axial position of the lower platen LP is given by the position of the lower tip of shaft N, which rests in the pan bearing of the leaf spring NS. At a constant speed of rotation of the lower platen LP, the specimen S is sheared at a constant and uniform shear rate $\dot{\gamma}_0$; S exerts a torque on the upper platen UP which twists the torsion bar TB. A linear displacement transducer T1 records this twist as a deflection which, after adequate calibration, represents the torque to be measured. The normal force existing in the specimen under test acts on the leaf spring NS. The servomotor SM lifts the free end of the leaf spring in such a way that the lower platen LP is always kept in the same position. At the free end of NS, a second

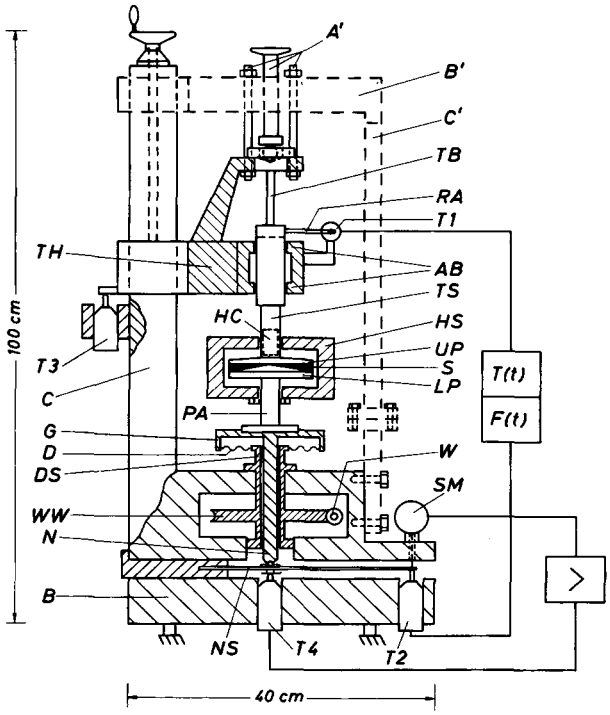

Fig. 1. Schematic diagram of the Weissenberg Rheogoniometer (WRG). Base B of the instrument with column C and torsion head TH. Rotating member: worm W, worm wheel WW, driving shaft DS, diaphragm D, gallery G with shaft N, platen adapter PA, and lower platen LP. Torsion head TH with torsion bar TB, torsion shaft TS, air bearing AB, and upper platen UP. Transducer T1 measures the deflection of radius arm RA. Normal force measuring system (commerical version): leaf spring NS, servomotor SM, transducers T2 and T4. HS and HC are two heating systems, transducer T3 is used for the gap setting after filling with specimen S. To improve mechanical stability, the traverse B' with a second column C' is added to the instrument. Screws A' clamp the upper end of torsion bar TB to the solid frame formed by B, B', C, and C'.

transducer T2 records the deflection representing the normal force F acting on the platen LP.

The shear stress p_{12} is related to torque T by[7]

$$p_{12} = 3T/2\pi R^3 \tag{1}$$

and the normal stress difference $p_{11} - p_{22}$ is calculated from the normal force F as follows:

$$p_{11} - p_{22} = 2F/\pi R^2 \tag{2}$$

where R is the radius of the gap.

The modifications which had to be made to the commercial version of the WRG consisted of improvements in the mechanical design, in the heating system, and in the ancillary electronic equipment.

For a reliable record of the transient normal force signal, it is necessary that the gap geometry be constant. A variation of the distance of the platens from each other during the test causes a flow in radial direction with the effect that the time-dependent normal stress record is incorrect. Such a "gap opening" is effected by a movement of each of the two platens. Under a thrust of 10 kgf, the upper platen of the original version of the WRG moved 10 μm ($\approx$400 microinches), which is considered to be too large (see normal force measurement discussion below). Therefore, a second column C′ with traverse B′ was attached to the instrument. The adjustable screw A′ with additional bolts provide a tight clamping of the upper end of the torsion bar TB. Traverse B′ and column C′ can be removed in order to fill the gap with the test specimen and to perform the "gap setting" (zero positioning). The introduction of B′ and C′ reduces the movement of the upper platen under load by more than the factor of 10.

A further important improvement of the mechanical part of the WRG consists of the replacement of the servo method for the normal force measuring device by a direct-indicating method. The servo system responds too slowly, resulting in "overshooting" and a nonstable signal at higher forces. In addition, when using the servo, the zero of the normal force record is not constant at higher temperatures. The direct-indicating method is described in more detail below. For the performance of the relaxation test, i.e., a stepwise rotation of the lower platen, an additional drive was developed which will be shown below.

To obtain an improved control of sample temperature, the commercial heating system had to be replaced. A variation of the sample temperature results in a variation of torque (since the viscosity of the material under test is temperature dependent) and, more seriously, in a variation of the "zero" of the normal-force signal, due to the thermal expansion of the specimen and apparatus. The new heating system consists of a main heater HS with a water jacket of thermostated temperature to prevent interaction with the (slightly varying) room temperature and of a second heater HC which compensates the heat flow along the torsion shaft TS. TS is cooled by the air of the air bearings AB which center the lower end of the torsion bar TB (Fig. 1). Special control circuits provide a constant sample temperature within $\pm$0.2°C (at 150°C) or better. The thermocouples used are calibrated in situ by a quartz thermometer (Hewlett-Packard, Model 2801). The main heater has a glass window for the observation of the free surface of the sample in the gap during the test. A nitrogen atmosphere protects the sample from being oxidized.

Figure 2 gives a general view of the rheogoniometer system. The mechanical part already described in Figure 1 can be protected against air draft by a box K which fits on cover K′. The drive unit consists of the synchronous motor DM, the variable transmission DH, and the gear box DGB. By means of a magnetic clutch DC, the rotation can be started and stopped suddenly. The variable transmission DH adjusts the input speed of the gear box in order to impose any desired shear rate to the specimen in a

wide shear rate range. For the control of the heaters, thermocouple compensators TCC are used together with galvanometers GA and GH. The torque and normal-force signals from the transducers T1 and T2 are amplified in A and recorded by different recorders depending on shear rate and total time of the measurement. It must be mentioned that the original transducers and amplifiers of the WRG had to be replaced by more stable and more accurate ones in order to keep the elastic deformation of the

Fig. 2. General view of the rheogoniometer system. In central part of the instrument, columns C, C′, the traverse B′, heater HS, and transducers T1 and T2 of Fig. 1 can be seen; K and K′ form a removable housing; T are heavy tables on which the instrument and the drive unit are mounted. Synchronous motor DM, variable transmission DH, gear box DGB form the drive unit which is connected by magnetic coupling DC to the instrument. A is the housing for the amplifiers the output of which can be recorded by XY, UV (ultraviolet), MR (multichannel strip-chart), TR (tape) recorders. TCC are two compensators for the thermocouple voltages; GA and GH are galvanometers for the heat control system. The resistors RR adjust the voltages for the heaters.

measuring springs of torque and normal force as small as possible ("hard apparatus").

In measuring polymer melts, the residence time of the material should be kept very short in order to minimize reactions in the specimen. On the other hand, due to the long relaxation times of polymer melts, a rather long waiting period may be required to attain the gap setting and the zero of the normal-force signal which corresponds to a stress-free initial state in the specimen. To shorten this period, premolded specimens are helpful, with dimensions which fit the cone-and-plate geometry of the test gap.

MEASUREMENTS IN THE LINEAR VISCOELASTIC RANGE

At sufficiently low constant shear rates $\dot{\gamma}_0$, polymer melts generate a torque which is proportional to the shear rate. In this "linear viscoelastic range" the "zero shear viscosity" η_0 can be measured directly[8]; η_0 is defined by

$$\eta_0 = \lim_{\substack{\dot{\gamma}_0 \to 0 \\ t \to \infty}} p_{12}(t)/\dot{\gamma}_0 \tag{3}$$

In measuring η_0, the growth curve of the shear stress characterizes the viscoelastic behavior of the material under test. Giesekus[9] denotes the ratio of the growing stress $p_{12}(t)$ over the (constant) shear rate $\dot{\gamma}_0$ as "stressing viscosity":

$$\eta(t) = p_{12}(t)/\dot{\gamma}_0 \tag{4}$$

The theory of linear viscoelasticity shows that in the linear viscoelastic region with $\eta^0(t)$ (the superscript zero indicates the linear viscoelastic range), stress growth, stress relaxation after cessation of steady shear flow, and shear relaxation modulus $G^0(t)$ are interrelated by the equations shown in Figure 3, where $\eta_0 = \lim_{t \to \infty} \eta^0(t)$, t' is the time measured from the cessation

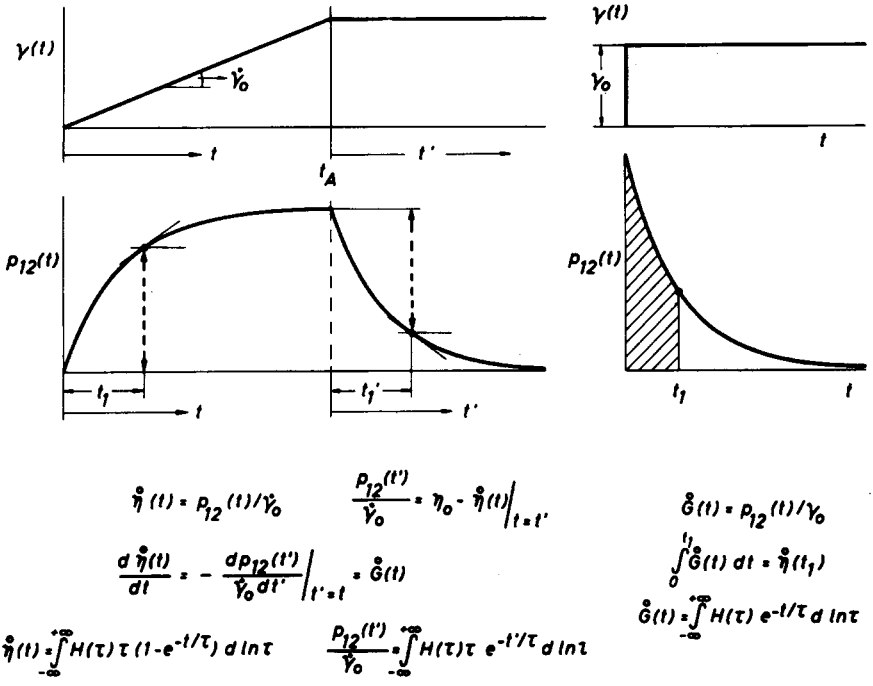

$$\dot{\eta}(t) = p_{12}(t)/\dot{\gamma}_0 \qquad \frac{p_{12}(t')}{\dot{\gamma}_0} = \eta_0 - \dot{\eta}(t)\Big|_{t=t'} \qquad \dot{G}(t) = p_{12}(t)/\gamma_0$$

$$\frac{d\,\dot{\eta}(t)}{dt} = -\frac{dp_{12}(t')}{\dot{\gamma}_0 dt'}\Big|_{t'=t} = \dot{G}(t) \qquad \int_0^{t_1} \dot{G}(t)\,dt = \dot{\eta}(t_1)$$

$$\dot{\eta}(t) = \int_{-\infty}^{+\infty} H(\tau)\,\tau\,(1-e^{-t/\tau})\,d\ln\tau \qquad \frac{p_{12}(t')}{\dot{\gamma}_0} = \int_{-\infty}^{+\infty} H(\tau)\,\tau\,e^{-t'/\tau}\,d\ln\tau \qquad \dot{G}(t) = \int_{-\infty}^{+\infty} H(\tau)\,e^{-t/\tau}\,d\ln\tau$$

Fig. 3. Relation between results of stress growth ("stressing") and stress relaxation experiment: t' is a new time base for the stress relaxation after cessation of steady flow. The linear viscoelastic material functions "stressing viscosity" $\eta^0(t)$ and stress relaxation modulus $G^0(t)$ are explained in text; $H(\tau)$ is the relaxation spectrum.[10]

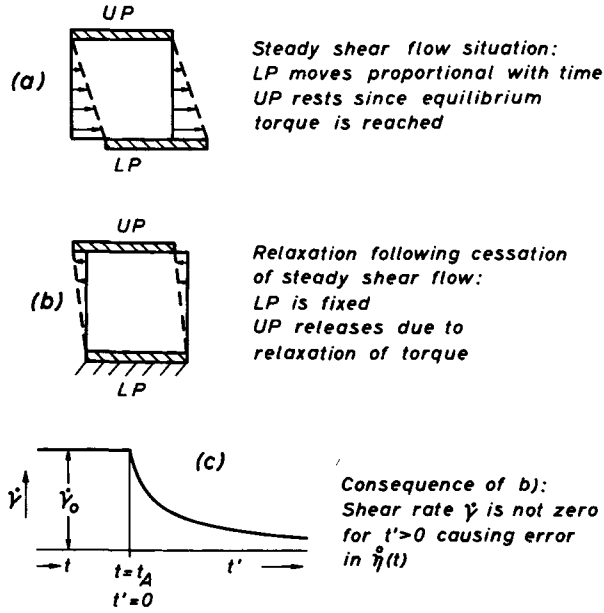

Fig. 4. Error in flow history caused by the elasticity of the torsion bar (TB of Fig. 1).

of steady shear flow, and $H(\tau)$ denotes the well-known relaxation spectrum.[10] It follows from Figure 3 that the linear viscoelastic behavior can be determined in a certain time range in measuring η_0 if the stress growth represents the time response of the material to the linear increase of the shear deformation $\gamma(t) = \dot{\gamma}_0 t$ only. However, the apparatus elasticity causes an error in $\gamma(t)$, since only the difference of the movements of the lower and the upper platen produces the shear in the specimen.

Figure 4 gives an example: In steady shear (a), the lower platen moves with constant speed to the right; the upper platen is at rest because the equilibrium torque is achieved. In (b), at a certain time $t' = 0$, the lower platen is stopped. For $t' > 0$, the material is not at rest due to the untwisting of the torsion bar which causes a movement of the upper platen to the left. This imposes a shear and consequently a shear rate on the melt, even for $t' > 0$ (c). Similarly, the ideal deformation histories in the stress growth and in the relaxation experiments are not achieved because of the elasticity of the torque-measuring device.

Constant Shear Rate (Stress Growth and Relaxation)

If a pretest indicates that, under the shear rate chosen, the material behavior is in the linear viscoelastic range and the material is chemically stable throughout the test, the stress relaxation measurement after cessation of steady shear flow is preferable to the stress growth measurement for the determination of $\eta^0(t)$ for the following reasons: (a) it is more difficult to determine $t = 0$ (start of stress growth) than $t' = 0$ (start of relaxation).

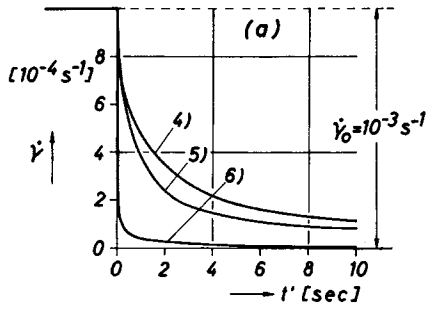

	gap		torsion bar		
arr.	α	diam. [mm]		diam. [mm]	length [mm]
4)	4°	72	T6	3.15	58
5)	6°	72	T6	3.15	58
6)	6°	72	T11	5.50	58

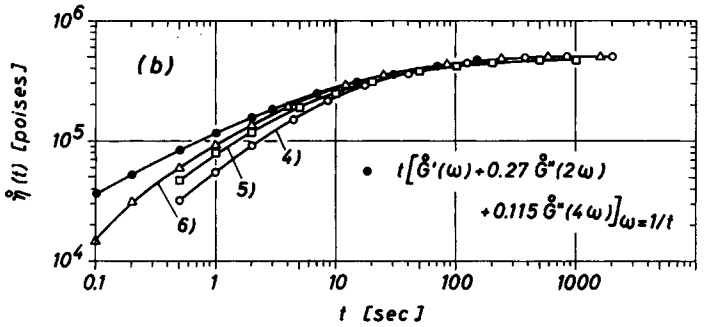

Fig. 5. Relaxation after steady shear flow: influence of gap and torsion bar dimensions on (a) true shear rate history and (b) stressing viscosity $\eta^0(t)$ calculated under the assumption of a stepwise cessation of the steady shear rate $\dot{\gamma}_0 = 0.001$ sec^{-1} at $t' = 0$. Specimen A (LDPE, $\rho_{20} = 0.918$ g/cm^3; Melt Flow Index[5] MFI = 1.4); temperature of measurement, 150°C.

(b) During the increase of the torque, the elastic deformation in the gear box and in the connecting shafts causes a lag in the rotation of the lower platen. Thus, an additional error arises which does not exist in relaxation since the drive is separated from the platen by the magnetic clutch. (c) During relaxation, the absence of vibrations from the drive unit gives a less noisy trace, and thus the variation of stress with time can be determined accurately over a longer period than is possible during stress growth.

Therefore, the following investigation of the influence of the elasticity of the torque-measuring device was made in stress relaxation after cessation of steady shear flow. Three different arrangements, 4, 5, and 6 (see table in Fig. 5), were chosen as combinations of two torsion bars (equal length, different diameter) and of two cone angles of the gap geometry. A shear rate $\dot{\gamma}_0 = 0.001$ sec^{-1} was applied to the specimen (material A at 150°C) until a constant torque was recorded (steady shear flow). At $t' = 0$, the magnetic clutch stopped the rotation of the lower platen. From the decay of the torque and from the elastic spring constant of the upper platen, the shear rate was calculated for $t' > 0$. The result is shown in Figure 5a. The torsion bar T6 was formerly used by us for the determination of η_0 of a melt

similar to material A.[8] It is remarkable that at $t' = 1$ sec, i.e., 1 sec after cessation of rotation, there is still a shear rate of about 40–50% of the former $\dot{\gamma}_0$ acting on the material. With the very thick torsion bar T11, still 5% of the original $\dot{\gamma}_0$ exists at $t' = 1$ sec. On the other hand, it seems to be desirable to know the time-dependent behavior from 0.1 sec on, because there are processing techniques in which the deformation of the polymer lasts much less than 1 sec.

With the usual evaluation of the stress decay signal, the three different arrangements deliver stressing viscosities which are shown in Figure 5b. The results coincide for long times t. In the transient short-time region, however, there are remarkable differences; the values assigned to $\eta^0(t)$ at a given value of t increase with increasing stiffness of the arrangement used. The filled circles are calculated from dynamic data using a formula which Dr. F. R. Schwarzl, T.N.O. Delft, kindly derived for us:

$$\eta^0(t)/t \approx \{G'(\omega) + 0.27\ G''(2\omega) + 0.115\ G''(4\omega)\}_{\omega=1/t} \qquad (5)$$

The relative maximum error of this equation is between $\pm 12\%$.[11] The dynamic data for specimen A were kindly provided by Dr. A. Zosel,[25] who used an oscillating cylinder viscometer in which the elasticity of the torque-measuring device was eliminated.[12] Therefore, the filled circles in Figure 5b represent values for $\eta^0(t)$ which would be obtained from an ideally stiff apparatus. It follows from Figure 5 that the elasticity of the apparatus has to be considered if the transient rheological properties are to be reliably measured in stress growth or stress relaxation after cessation of steady shear flow.

Stress Relaxation

For the relaxation test, an additional drive (Fig. 6) was developed to enable the lower platen rotation to be started and stopped suddenly. This drive consists of a ring system which can be mounted to the base of the apparatus, and of a new torsion shaft TS and gallery G which can freely rotate within the shaft DS of Figure 1. Around G, a ring RG is mounted which is connected with two force springs SFC applying a couple. When the springs are stressed, a ball in RG is pressed against the stop S2 of the ring system shown at the right-hand side of Figure 6. Stop S2 is fixed to the inner ring RI which can freely rotate; the outer ring RO is fixed to the base of the WRG. In stressing the springs SFC, the rotation of RI can be prevented by a bolt SS. If SS is released, the inner ring RI rotates through a small angle which is preset, being determined by the distance between the stops S1 and S1′. In order to study the movement of the lower platen, two linear displacement transducers T can be used which are mounted to G. The total angle of rotation (and therefore the total shear strain) can be measured in addition optically by mirror M.

Two principal errors arise in the relaxation test: (a) the step function of the shear strain has a nonzero rise time; (b) the sudden rotation of the lower platen is only partly used for the shear strain step γ_0 and partly for

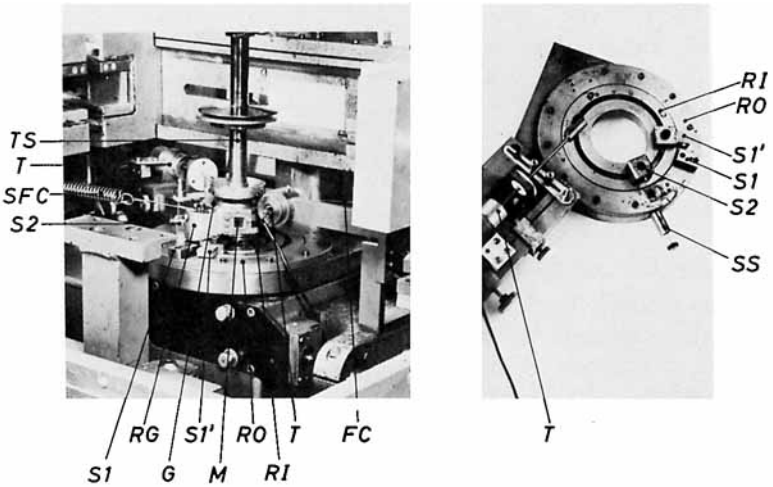

Fig. 6. Additional equipment for the shear relaxation test. The right-hand photograph is a view from the top of the ring system which is mounted to the WRG in the left-hand picture. Column C′ of Fig. 1 and Fig. 2 is removed and the heater is opened in order that the two platens forming the cone-and-plate gap can be seen. Torsion shaft TS with gallery G and ring RG, RI inner, RO outer ring with stops S1, S1′, S2, and SS. Linear displacement transducer T, coil spring SFC, connection FC to a second (invisible) coil spring; both coil springs exert a couple on G. Mirror M is mounted to G.

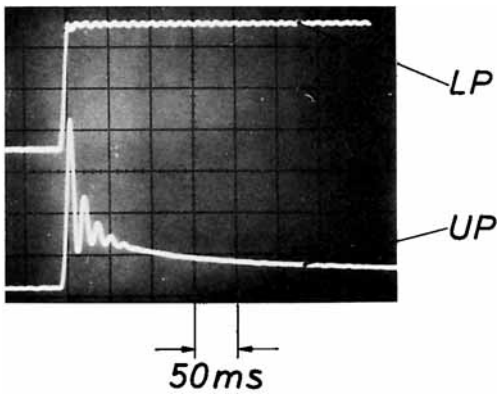

Fig. 7. Time-dependent deflection of the lower platen LP and the upper platen UP in the relaxation test using the equipment of Fig. 6, with torsion bar T8 (58 mm long, 8.90 mm diameter) and a gap of 72 mm diameter and $\alpha = 4$ degrees. Material A, 150°C; ordinate: deflection of the platens; abscissa: time.

the twist of the torsion bar which untwists in course of time because of the relaxation of the material. Fortunately, very thick torsion bars can be used such that, in practice, for $t > 0.1$ sec these principal errors can be neglected.

The influence of the apparatus elasticity on the stress relaxation modulus of material A was investigated using three arrangements of torsion bars and gap geometries. No systematic difference in the results for $t > 0.1$ sec could

be detected. For one of these arrangements with torsion bar T8 (length 58 mm, diameter 8.90 mm) and a gap of 72 mm diameter and of 4 degrees cone angle, the movements of the two platens at the beginning of the relaxation test were studied using a twin-channel electron-beam oscillograph. The result is shown in Figure 7. Apparently, the rise time of the lower platen movement is about 10 msec. Following a rule-of-thumb of linear viscoelasticity, the stress decay for times longer than ten times the rise time represents, to a sufficient approximation, the response to an ideal stepwise deformation. The trace of the upper platen movement indicates a superimposed oscillation caused by the momentum at the start of the test. However, this oscillation is damped rapidly, and reliable data can be taken for times $t > 100$ msec $= 0.1$ sec.

Relations Between Linear Viscoelastic Material Functions

The relaxations modulus $G^0(t)$ of material A at 150°C is shown in Figure 8 together with the dynamic functions G' and G'' plotted versus $1/\omega$. $G^0(t)$ was determined in different ways: (a) by direct measurement in the relaxation test, i.e., stress relaxation after a stepwise total shear strain γ_0 with γ_0

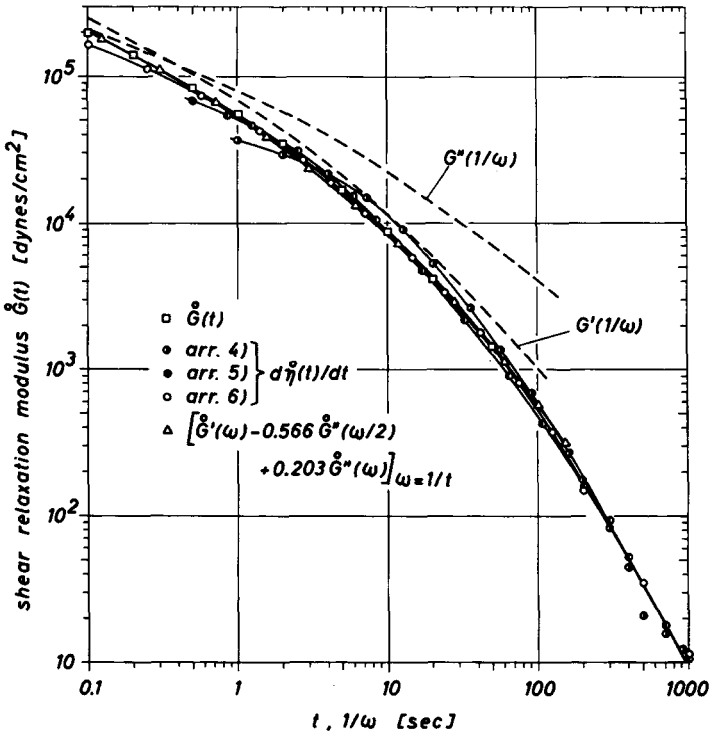

Fig. 8. Shear relaxation modulus $G^0(t)$ of specimen A determined by different methods: (a) measured directly, (b) calculated as the slope of the stressing viscosity $\eta^0(t)$ using different arrangements, compare Fig. 5, and (c) calculated from storage and loss moduli using eq. (6). Test temperature 150°C.

<0.5. As has been shown recently[1] for a melt similar to specimen A, the relaxation modulus is independent of γ_0 for γ_0 <0.5; (b) from the derivative of the stressing viscosity, $G^0(t) = d\eta^0/dt$ (compare the equations of Fig. 3); and (c) from the storage modulus $G'(\omega)$ and loss modulus $G''(\omega)$ using the formula[13]

$$G^0(t) = \{G'(\omega) - 0.566\ G''(\omega/2) + 0.203\ G''(\omega)\}_{\omega=1/t} \qquad (6)$$

It follows from Figure 8 that the directly measured curve (a) coincides perfectly with the one calculated from the dynamic data (c) using eq. (6) for t >0.1 sec. The disadvantage of the direct method (a) is that the modulus can be measured only up to t = 50 sec. Moreover, dynamic measurements with ω <0.01 sec^{-1} are difficult to perform. The slope of the stressing viscosity curve (b) allows one to extend the time scale for one more decade (up to 1000 sec) and the range of modulus for two more decades. This is a consequence of the different stress decay in relaxation after a stepwise shear or after cessation of steady shear flow. The difference in stress decay follows already from the fact that the two material functions, $G^0(t)$ and $\eta^0(t)$, are related to the relaxation spectrum $H(\tau)$ in different ways (equations of Fig. 3). However, the derivative of the stressing viscosity agrees with the shear relaxation modulus only if $\eta^0(t)$ is measured by means of a very stiff device. Even the data from the stiffest arrangement 6) of Figure 5 do not give a derivative which agrees with $G^0(t)$ for t <0.5 sec. On the other hand, it is remarkable that the stressing experiment (stress growth or stress relaxation after cessation of steady shear flow), if it is performed carefully, does provide not only the zero shear viscosity η_0 but in addition the relaxation modulus $G^0(t)$ in the wide range of four decades from 10^5 to 10 dynes/cm^2.

A second important result following from Figure 8 is that the relations of the theory of linear viscoelasticity apply to molten polymers if the total deformation, or deformation rate, is sufficiently small.

MEASUREMENTS IN THE NONLINEAR REGION

At higher rates of shear, polymer melts show large normal stresses and pronounced maxima in the variations of shear stress and normal force with time. This was shown first for molten polyethylene in 1955 by Pollett.[14]

The commercial version of the WRG seems to be quite incapable of yielding reliable normal force data for polymer melts. The main reason is that in polymer melts (except at very low shear rates), the normal forces are so high and grow so quickly that the servo system cannot follow them. In consequence, there is a periodic gap opening and a large-amplitude periodic variation of the normal force. The latter shows up as a "saw-tooth" trace, whose minima are near zero and whose maxima are very high reflecting the properties of the measuring system and not of the material. For such materials, this normal force system can be used neither for transient nor for steady-state measurements.

In this section, a new direct-indicating normal-force measuring system is described and the influence of the gap dimensions on the records obtained is discussed. Finally, for a wide range of constant shear rates, transient shear and normal stress data are given which are believed to represent rheological properties of the material under test, uninfluenced by the apparatus.

Normal-Force Measuring System

The direct indicating system for the measurement of normal forces is shown in Figure 9. The notation corresponds to that of Figure 1. The lower platen LP together with the gallery G rests on the lower tip of shaft N, which acts on leaf spring NS at bearing BB. Compared with the springs of the former servo system, the active length of the new spring is much smaller and the shaft CS (clamped to the base of the WRG) is much longer.

The slope of the spring at $x = a$ is determined from the measured values of the deflection (at $x = l$) of a rigid arm A which is made of a thin-walled aluminium profile. The outer end of A (at $x = l$) is attached to the core C of a linear displacement transducer T2. The transducer housing is rigidly attached to the shaft CS by means of the connection A'. Thus the elastic element NS including the moving indicator C and the fixed reference T2 are both connected with the WRG at the same point of the WRG base. This type of connection improves the zero-stability of the normal-force measuring device remarkably.

Three different normal force springs for different ranges were designed in such a way that, for each spring, the maximum load F_{max} corresponds to a deflection $s = 1$ μm ($\approx$40 microinches) at $x = a$. The corresponding values of the deflection f, measured by the transducer at $x = l$, are listed in Figure 9 together with the dimensions of the springs. It is seen that a mechanical amplification of 15 or 30 is obtained. The accuracy of the normal force measurement is $\Delta F/F_{max} \leqq 0.005$. This corresponds to an axial movement $\Delta s = 0.005$ μm ($\backsimeq$0.2 microinches), which may be caused by temperature variations in the specimen or in the rheogoniometer or, more probably, by a slight roughness in the bearing BB for which the same design was used as in the commercial version of the WRG.

The deflection of the leaf spring necessarily involves an opening of the cone-and-plate gap (1 μm under the maximum load F_{max}). With this must be associated a radial flow of the material under test. If the normal forces grow quickly and the resistance to this radial flow is high, a delay in the normal force response will occur. To investigate these effects, normal force and shear stress measurements were made at the same shear rate using different gap diameters and angles. It was found that, as expected, the delay shown by the normal force record increased with increasing gap diameter. Accordingly, the influence of cone angle changes was investigated more fully, using the relatively small gap diameter of 24 mm.

Figure 10 shows the result of a test series performed at a shear rate of 10 sec^{-1}. For these tests, the "hardest" torsion bar (T8 with an 8.9-mm

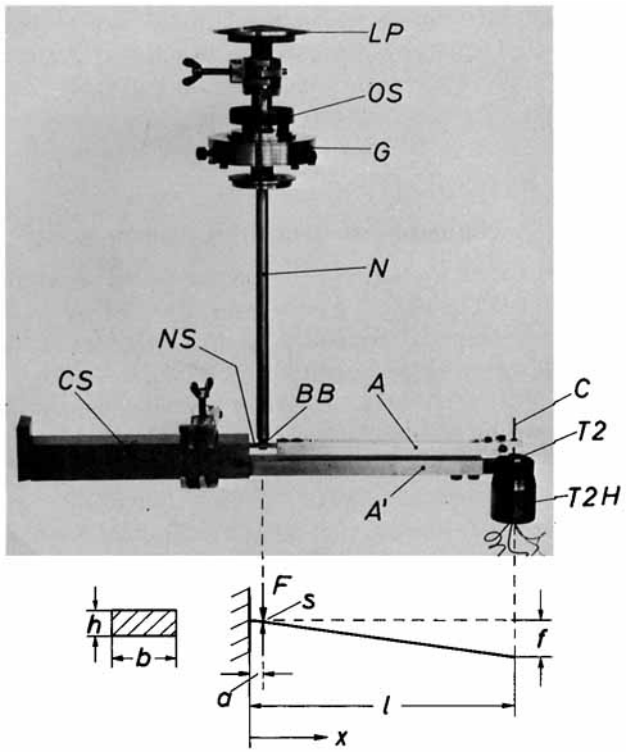

	F_{max} [kgf]	a	l	b	h	s	f
		[mm]				[μm]	
P6	10	20	210	20	9.8	1	15
P7	2	10	200	10	3.3	1	30
P8	0.5	10	200	8	2.25	1	30

Fig. 9. Direct-indicating system for measurement of normal forces. Lower platen LP of cone-and-plate gap; gallery G, normal force shaft N (compare Fig. 1) which fits into bearing BB, oil seal OS which prevents draft in heater. Shaft CS clamped to the WRG base, leaf spring NS. Arm A connects core C of transducer T2 to NS; arm A′ connects CS and the housing T2H of the transducer. The active length a of spring NS is very short; the small deflection s at $x = a$ is amplified mechanically and measured as displacement at $x = l$. The table shows the dimensions of the three springs used with maximum loads F_{max} which correspond to a maximum deflection $s = 1\ \mu m$; b and h are the dimensions of the rectangular cross section of NS.

diameter) and the hardest normal force spring (P6, see Fig. 9) were used. The normal forces F and the torques T of Figure 10 are multiplied by factors occurring in eqs. (2) and (1), respectively.

The most striking result following from Figure 10 is the remarkable influence of cone angle α on the time dependence of the normal force signal, indicating that with the "usual" cone angles (4 degrees and smaller) the

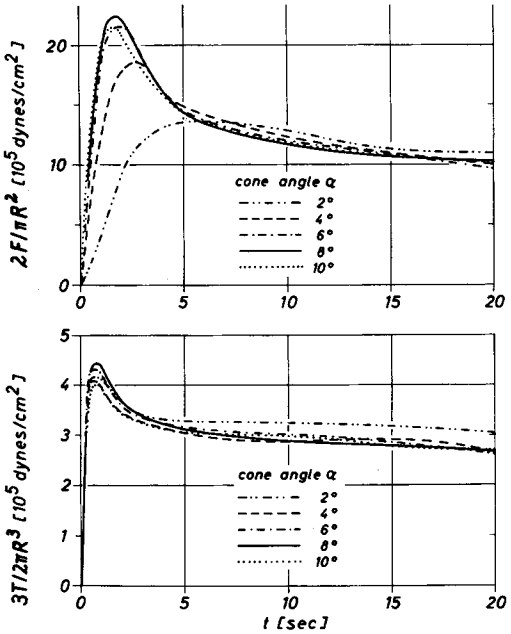

Fig. 10. Normal force F (top) and torque T (bottom) as a function of time at constant shear rate $\dot{\gamma}_0 = 10\ \text{sec}^{-1}$: specimen A at 150°C. The tests were performed with a gap diameter of 24 mm and different "cone angles" α (angle between the flat platen and the cone forming the gap). In these graphs, F and T are multiplied by factors which occur in eqs. (2) and (1), respectively.

test result reflect both material and apparatus properties. Only the records for $\alpha = 6$, 8, and 10 degrees coincide within the reproducibility of the measurement. Consequently, only these normal force curves can be attributed to the normal stress difference $p_{11} - p_{22}$. The curves of the torque are not influenced by cone angle α within the range of α used, except for the case $\alpha = 2$ degrees, where the slowly decreasing part of the curve after the maximum is more nearly horizontal than for the other cone angles.

Because of the results of Figure 10, a cone angle of $\alpha = 8$ degrees, and a gap diameter of 24 mm were chosen as the "standard gap" for the following experiments which were performed with constant shear rates ranging from 0.01 to 50 sec^{-1}.

Influence of Shear Rate on Time Dependence of Shear Stress and First Normal Stress Difference

The records of Figure 10 for $\alpha = 6$–10 degrees indicate pronounced maxima in the first normal stress difference $p_{11} - p_{22}$ and in the shear stress p_{12} as well. Beyond the maxima, both functions decrease steadily, and therefore the questions arise whether an equilibrium state of stress, or, in other words, a steady state of flow, really does exist and, if it does, how long the material must be sheared in order to achieve this steady-state flow.

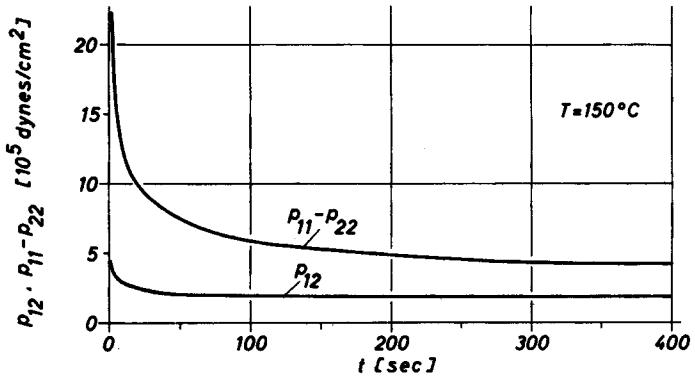

Fig. 11. Shear stress p_{12} and first normal stress difference $p_{11} - p_{22}$ as a function of time (linear time scale) measured at a shear rate of $\dot{\gamma}_0 = 10$ sec^{-1} at a temperature of 150°C. Standard gap (24 mm diameter, cone angle $\alpha = 8$ degrees), material A.

For material A, the answer is given in Figure 11, where the two functions are shown over a longer time scale. The test from which these results were taken was performed with the same shear rate $\dot{\gamma}_0 = 10$ sec^{-1} using the standard gap, but the shear action lasted much longer than during the tests of Figure 10. In Figure 11, the maxima seem to be more pronounced since especially the normal stress curve decreases much more than in Figure 10 until the horizontal part of the curve is achieved at a total duration of shear of about 300–400 sec. The maxima are built up quickly at the very beginning of the shear action followed by a stress decrease which lasts a remarkably long time until the equilibrium stress corresponding to the steady state is reached.

The details of the transient functions can be seen more clearly especially in the short-time region if a logarithmic scale is used (Fig. 12). Here, the curves for $\dot{\gamma}_0 = 10$ sec^{-1} are replotted, and additional results for $\dot{\gamma}_0 = 1$, 2, and 5 sec^{-1} are shown. It follows from Figure 12 that, with increasing shear rate, the maxima of p_{12} and of $p_{11} - p_{22}$ increase and that these maxima occur at earlier times. It turns out that the maximum of each function is connected with a definite constant total shear $\gamma = \dot{\gamma}_0 t$, which is independent of shear rate but is different for shear stress and normal stress difference. In fact, the maximum of $p_{11} - p_{22}$ occurs distinctly later than the maximum of p_{12}. In this context, the results of Malkin, Yarlykov, and Vinogradov[15] must be mentioned; they showed that the recoverable part of the total strain (measured in a recovery experiment) still increased shortly after the maximum of the shear stress was attained. The steeply increasing normal force signal in the decay region of the shear stress just after $p_{12,\max}$ supports their result, see eq. (7), below.

In order to discuss the shear rate dependence, it is convenient to define certain parameters for the transient behavior observed in a constant shear-rate experiment. For this purpose, we shall use the maxima of shear stress

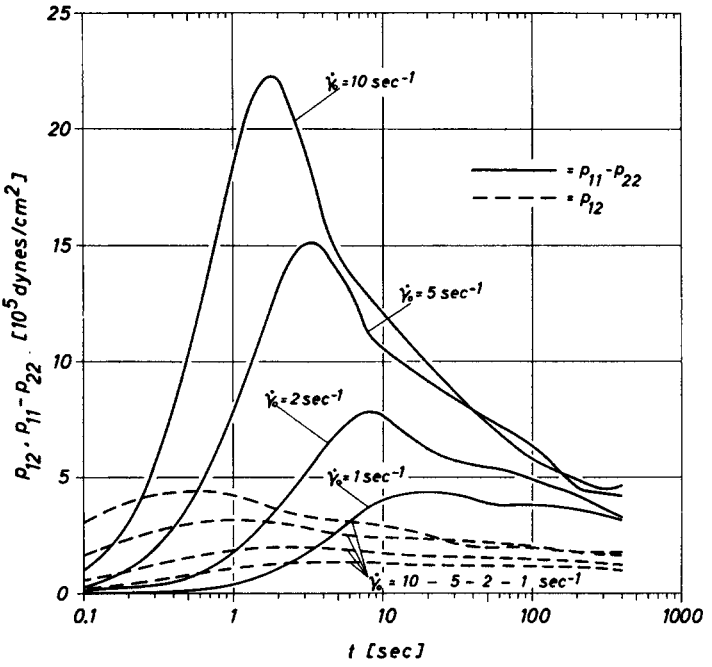

Fig. 12. Transient stress functions p_{12} and $p_{11} - p_{22}$ for different constant shear rates $\dot{\gamma}_0$ plotted vs. a logarithmic time scale. Standard gap, material A, temperature T = 150°C.

$p_{12,max}$ and of normal stress difference $(p_{11} - p_{22})_{max}$. In addition, we shall use the values of p_{12} and $p_{11} - p_{22}$ at the times t = 100, 200, and 400 sec in order to characterize the approach to steady flow (see Fig. 11).

Figure 13 gives the parameters selected as a function of shear rate in double logarithmic coordinates. At low shear rates, there is no time dependence at all: the different curves for the shear stress practically coincide and so do the curves for the normal stress difference. At $\dot{\gamma}_0 = 0.01$ sec^{-1}, the slope is less than 1 for p_{12} and less than 2 for $p_{11} - p_{22}$, indicating that the material does not behave like a second-order fluid in the whole range of $\dot{\gamma}_0$ studied. For $\dot{\gamma}_0 > 0.5$ sec^{-1}, the values of the maxima increase steadily with a slightly decreasing slope, but the values for t = 100, 200, and 400 sec increase less rapidly with increasing $\dot{\gamma}_0$ and become constant for $\dot{\gamma}_0 \geqq 8$ sec^{-1}. The decrease of p_{12} for $\dot{\gamma}_0 > 10$ sec^{-1} and t = 100–400 sec is ignored in the further discussion.

Two important results follow from Figure 13: (a) the maximum of the state of stress increases steadily with shear rate, whereas (b) the equilibrium stress increases much less until (at about $\dot{\gamma}_0$ = 8 sec^{-1}) a final value is achieved which is independent of shear rate. Correspondingly, the ratio of the maximum and of the equilibrium values of stress increases: at $\dot{\gamma}_0$ = 50 sec^{-1}, this ratio is about 10 for $p_{11} - p_{22}$.

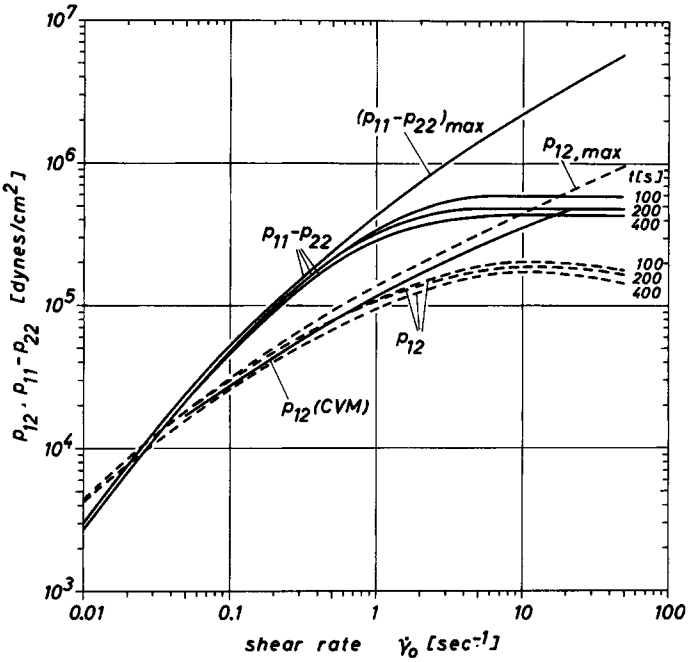

Fig. 13. Parameters of the transient records of shear stress p_{12} and first normal stress difference $p_{11} - p_{22}$ as functions of shear rate. The parameters represent the maxima and the values at times t = 100, 200, and 400 sec. CVM gives the shear stress obtained from capillary viscometer data using corrections for true shear rate (Weissenberg) and true shear stress (Bagley). Material A at 150°C.

Figure 13 also shows the shear stress as a function of shear rate measured in a capillary viscometer using the Weissenberg correction[16] for true shear rate and Bagley's plots[17] for the determination of the true shear stress. It turns out that the capillary data coincide sufficiently with the WRG shear stress if the shear rate is low enough. At higher shear rates, the capillary results lie between the maximum and the equilibrium values of the time-dependent shear stress. This result can be understood in the light of Figure 11, which shows that the maximum in the shear stress occurs very quickly. In the capillary experiment, a typical fluid element presumably attains its maximum shear stress just before entering the die. Its subsequent behavior, which governs the measured viscosity, thus represents a time average of the values of p_{12} shown in Figure 11.

It has been mentioned already that, in elastic liquids, the shear flow is connected with an elastic, recoverable shear strain γ_R which is related to the stress ratio

$$\Gamma = (p_{11} - p_{22})/p_{12} \tag{7}$$

such that $\gamma_R = \Gamma$, if the material under test fulfills the equation of the so-called "neo-Hookean theory of elastic deformation" formulated for solids by Rivlin.[18] The alternative relation $\gamma_R = 0.5\Gamma$ was derived by Lodge[19]

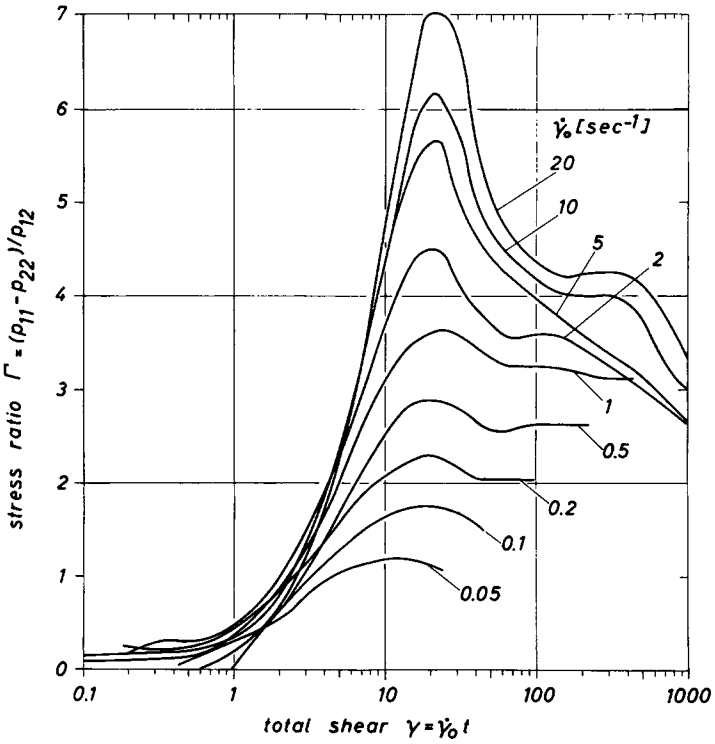

Fig. 14. Stress ratio $\Gamma = (p_{11} - p_{22})/p_{12}$ as a function of total shear strain $\gamma = \dot{\gamma}_0 t$ at different shear rates $\dot{\gamma}_0$. Material A, $T = 150°C$, standard gap.

for the "rubberlike liquid" model,[20] where in this case Γ denotes the equilibrium value in steady shear flow.

Figure 14 represents the stress ratio Γ as a function of the total shear strain $\gamma = \dot{\gamma}_0 t$. The onset of the growth of Γ is approximately equal for all shear rates. It is obvious from this figure that the maxima of the curves $\Gamma(\gamma)$ are located at a total shear strain of about $\gamma = 22$, independent of shear rate. At high shear rates, the shape of the curves in the neighborhood of the maxima is nearly symmetric; at the highest shear rates, the existence of a less-pronounced second maximum is indicated. For the discussion of Figure 14, it should be observed that the same distance on the abscissa belongs to a different instant of time for each curve.

The maxima of the state of stress and of the stress ratio Γ (related to the recoverable shear strain) indicate that a much greater resistance against shear flow does exist during the "prestationary region" in the material under test than in the steady-state equilibrium. The maxima are evidence of a remarkable hindrance which is overcome during the shear deformation. There is no breakage of chemical bonds, and the hindrance is built up again rather quickly when the deformation rate is ceased: If a second shear experiment follows immediately the complete relaxation of shear stress and normal stress components after cessation of a first shear experiment

with the same shear rate, again the maxima of the recorded functions are found comparable in magnitude to the results of the first run.

COMPARISON OF SHEAR AND TENSILE DATA

Tensile tests with material A at 150°C were made with an apparatus already described.[21] The results confirm the general extensional behavior of LDPE melts.[22] Analogous to eq. (4), a "stressing viscosity in extension" $\mu(t)$ is defined by

$$\mu(t) = \frac{p_{11}(t) - p_{22}(t)}{\dot{\epsilon}_0} \tag{8}$$

where the tensile stresses p_{11} and p_{22} are parallel and normal to the flow direction, respectively, and $\dot{\epsilon}_0$ is the constant Hencky strain rate applied to the specimen under test. For the linear viscoelastic case, the notation $\mu^0(t)$ is used, and it was shown recently[22] that the relation

$$\mu^0(t) = 3\eta^0(t) \tag{9}$$

is valid for the linear viscoelastic case. Using this factor 3 originally found by Trouton,[23] the Schwarzl formula, eq. (5), can be applied to determine the linear viscoelastic stressing viscosity in extension from shear dynamic data.

In Figure 15, the stressing viscosities in shear and in extension are plotted as functions of time for a wide range of shear rates ($\dot{\gamma}_0 = 0.001$ to 20 sec^{-1}) and elongation rates ($\dot{\epsilon}_0 = 0.001$ to 1 sec^{-1}). If allowance is made for the scatter in the data and for the spread of shear data near 0.1 sec (which, as discussed above, is due to apparatus limitations), then the following conclusions can be drawn from the data of Figure 15:

1. In shear, the curve for the linear viscoelastic case, i.e., $\eta^0(t)$ according to the Schwarzl formula, eq. (5), represents the envelope for the stressing viscosities $\eta(t)$ obtained for all shear rates. With increasing shear rate, $\eta(t)$ deviates earlier from $\eta^0(t)$ and shows a maximum, which occurs at a shear strain almost independent of shear rate $\dot{\gamma}_0$.

2. In extension, for small total strains up to $\epsilon \approx 1$, the stressing viscosity $\mu(t)$ follows that for the linear viscoelastic case, $\mu^0(t) = 3\ \eta^0(t)$. Then a rapid increase follows, the onset of which seems to occur at a constant total strain nearly independent of strain rate $\dot{\epsilon}_0$. In contrast to the well-known shear thinning or "work softening" in shear, there is a pronounced "work hardening" in extension.

3. Comparing the extensional and the shear behavior, the factor 3 in eq. (9) is confirmed for the linear viscoelastic case, i.e., for low strain rates or small total strains. The most important result following from Figure 15 is that at higher strain rates and larger total strains, the behavior is strikingly different, namely, increase in viscosity in extension but decreasing viscosity in shear. We note that in both types of deformation the deviation from the linear viscoelastic limiting case occurs approximately at a constant magnitude of the deformation, independent of deformation rate. In comparing

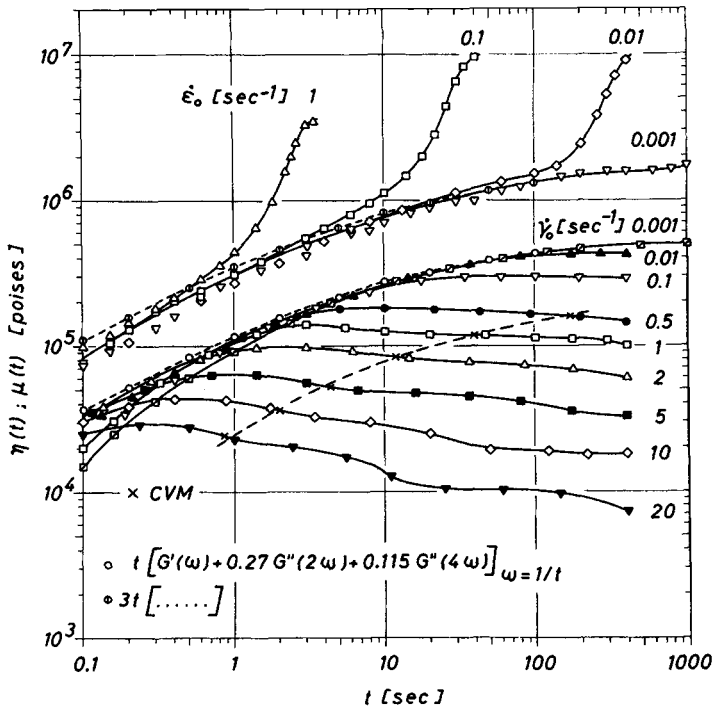

Fig. 15. Stressing viscosity in shear $\eta(t)$ and in extension $\mu(t)$ at different deformation rates. Material A, T = 150°C: (o) data calculated from dynamic data using eq. (5); (x) capillary viscometer (CVM) data plotted in this graph at times t at which the viscosity, measured in the CVM, coincides with $\eta(t)$, measured in the WRG, for the shear rates indicated.

such data for shear flow and elongational flow, two points should be kept in mind: (a) the elongation viscosity $\mu(t)$ is calculated from a difference of principal stresses, whereas the shear viscosity $\eta(t)$ is calculated from a single stress component p_{12}, and not from a difference of principal stresses which would involve both $p_{11} - p_{22}$ and p_{12}; and (b) the principal elongation ratios, measured from the initial state, have very different time dependences in the two types of flow.

4. For a polymer melt having such pronounced time-dependent properties as specimen A, the capillary viscometer data (even when corrected as described above) yield values for "viscosity" which differ greatly from the values of the ratio of shear stress to shear rate obtained under steady shear flow conditions. The viscosity data obtained from the capillary viscometer fit to a single point of each of the time-dependent shear viscosity curves of Figure 15. These points are always located at the right of the maxima of the curves. This can be attributed to the pronounced entrance region of the LDPE melt in capillary flow, such that a flowing material element is stressed most in front of the die entrance. The tremendous time dependence of the recovery (recoverable shear strain), which is suggested by the

steep drop in the stress ratio Γ after its maximum (Fig. 14), is presumably associated in capillary flow with the pronounced dependence of extrudate swell on the length of the capillary.[1]

FINAL REMARKS

The final conclusions of the last section summarize the behavior of the LDPE sample at 150°C in shear and in extension. With respect to the apparatus, the results show that the rheogoniometer can in fact be modified to yield reliable data for the time-dependent shear stress and first normal stress difference at constant shear rate. It is essential, however, to check for the specific material under test whether the dimensions of the gap geometry do yield "geometry independent" results.

In future, the second normal stress difference, $p_{22} - p_{33}$, should be determined from the data already obtained and from additional measurements in a gap formed by two parallel platens.[24] With respect to the experimental development, an automatic processing of the WRG data is highly desirable.

It is a great pleasure for me to thank Messrs. R. Benz and M. Reuther for their help in the improvement of the rheogoniometer, for the performance of the tests, and for the evaluation of the data. I also like to express my thanks to Dr. F. R. Schwarzl, T.N.O. Delft, for communicating eq. (5) to me in advance of publication, to my colleague Dr. A. Zosel for the measurement of the dynamic functions $G'(\omega)$ and $G''(\omega)$ of material A, and to Prof. A. S. Lodge, Madison, Wisconsin, for many helpful discussions concerning the subject of this paper.

References

1. J. Meissner, *Kunststoffe*, **61**, 576 and 688 (1971).
2. K. Weissenberg, *The Testing of Materials by Means of the Rheogoniometer*, Farol Research Engineers, Bognor Regis, Sussex, England, 1964.
3. J. L. S. Wales, *Pure Appl. Chem.*, **20**, 331 (1969).
4. J. Meissner, in preparation.
5. Melt Flow Index MFI 190/2.16, German Standard DIN 53735, U. S. Standard ASTM D 1238-65 T.
6. A. Jobling and J. E. Roberts, *J. Polym. Sci.*, **36**, 421 (1959).
7. B. D. Coleman, H. Markovitz, and W. Noll, *Viscometric Flows of Non-Newtonian Fluids*, Springer, Berlin/Heidelberg/New York, 1966.
8. J. Meissner, in *Proc. Fourth International Congress on Rheology, Providence*, 1963, Part 3, Interscience, New York, 1965, p. 437.
9. H. Giesekus, *ibid.*, p. 15.
10. J. D. Ferry, *Viscoelastic Properties of Polymers*, 2nd ed., Wiley, New York, 1970.
11. F. R. Schwarzl, private communication 1970.
12. J. L. denOtter, *Rheol. Acta*, **8**, 355 (1969).
13. F. R. Schwarzl, *Pure Appl. Chem.*, **23**, 219 (1970).
14. W. F. O. Pollett, *Brit. J. Appl. Phys.*, **6**, 199 (1955).
15. A. Ya. Malkin, B. V. Yarlykov, and G. V. Vinogradov, *Rheol. Acta*, **9**, 329 (1970).
16. R. Eisenschitz, B. Rabinowitsch, and K. Weissenberg, *Mitt. Deutsch. Material-Prüf-Anst., Sonderheft 9*, 91 (1929).
17. E. B. Bagley, *J. Appl. Phys.*, **28**, 624 (1957).
18. R. S. Rivlin, *Phil. Trans. Roy. Soc.*, **A240**, 459 (1948).
19. A. S. Lodge, *Rheol. Acta*, **1**, 158 (1958).

20. A. S. Lodge, *Elastic Liquids*, Academic Press, London, 1964.
21. J. Meissner, *Rheol. Acta*, **8**, 78 (1969).
22. J. Meissner, *Rheol. Acta*, **10**, 230 (1971).
23. F. T. Trouton, *Proc. Roy. Soc.*, **A77**, 426 (1906).
24. T. Kotaka, M. Kurata, and M. Tamura, *J. Appl. Phys.*, **30**, 1705 (1959).
25. A. Zosel, unpublished data.

Received February 3, 1972
Revised May 30, 1972